communications biology

A Nature Portfolio journal

Article

https://doi.org/10.1038/s42003-025-07897-0

ZDHHC9-mediated CD38 palmitoylation stabilizes CD38 expression and promotes pancreatic cancer growth

Hui Guo[1,2,3], Zhiqing Lin[1,3], Di Zhang[1,3], Qilong Qin[1], Zewen Li[1], Yuqing Yin[1], Jiangfan Chen[1,2] ✉ & Wei Guo[1,2] ✉

The cluster of differentiation 38 (CD38) is a multifunctional transmembrane protein involved in numerous physiological and pathological processes including aging, neurodegenerative diseases, and tumorigenesis, hence is an attractive drug target. However, the mechanisms underlying the regulation of CD38 expression remain enigmatic. Herein, we report for the first time that CD38 is palmitoylated at Cys16, and that S-palmitoylation is required to maintain CD38 protein expression in tumor cells. Furthermore, we identify DHHC9 as the palmitoyl transferase and APT1 as the acylprotein thioesterase responsible for this crucial post-translational modification. Finally, we designed a competitive peptide of CD38 palmitoylation that decreases CD38 expression in tumor cells and suppresses tumor progression in vivo. These findings provide novel insight into CD38 regulation and highlight potential therapeutic strategies targeting CD38 palmitoylation for cancer treatment.

Cluster of differentiation 38 (CD38), a multifunctional type II transmembrane glycoprotein, is involved in several physiological and pathological conditions, including aging[1,2], neurodegenerative diseases[3], social behavior[4] and tumorigenesis[5–7]. As an ectoenzyme, CD38 exhibits both NAD^+ glycohydrolase and ADP-ribosyl cyclase activities, allowing it to cleave NAD^+ into cADPR and ADPR, which are involved in the mobilization of Ca^{2+} from intracellular stores[8–10]. In addition to its enzymatic function, CD38, which is a receptor for CD31, plays a crucial role in the regulation of cell migration, signal transduction, and receptor-mediated adhesion[11]. CD38 is highly expressed in hematological malignancies such as multiple myeloma (MM), whereas it has relatively low expression in non-hematopoietic tissues, making it an attractive therapeutic target for hematological malignancies[12]. In particular, several CD38 antibodies are currently undergoing clinical trials for the treatment of $CD38^+$ malignancies, among which daratumumab and isatuximab have received the approval of the Food and Drug Administration (FDA) for the treatment of multiple myeloma[13,14]. Therefore, CD38 is identified as a key drug target that warrants further investigation.

The expression of CD38 is markedly upregulated in cancers; however, the underlying regulatory mechanisms remain largely undefined. Previous studies have determined that CD38 expression is regulated by several factors such as LXR, NF-κB, STAT and other transcription factors. For example, TNF-a induces CD38 expression in human airway smooth muscle cells through the activation of transcription factors like NF-κB and AP-1[15,16]. Additionally, in monocytes and chronic lymphocytic leukemia (CLL) cells, treatment with IFN-γ produced upregulation of CD38 expression via IRF-1 and STAT transcriptional activation of the CD38 promoter[17–19]. Furthermore, activation of the LXR signaling pathway enhances CD38 expression, contributing to the defense of host macrophages against bacterial infection[20]. These findings mainly focus on the regulation of CD38 gene transcription levels. However, whether other mechanisms, such as post-translational modifications regulate the expression of CD38 remain to be further understood.

Palmitoylation, specifically S-palmitoylation, is the only reversible protein-lipid modification, which involves the attachment of the 16 carbon fatty acid palmitate to cysteine residues in substrate proteins through a thioester bond[21], and these intracellular palmitoylation reactions are mediated by a large family of aspartate-histidine-histidine-cysteine (DHHC or ZDHHC) palmitoyl transferases. Palmitoylation virtually alters cellular function by regulating substrate structure, stability, subcellular localization, protein–protein interactions, and signal transduction[22–24]. In particular, palmitoyl transferases are crucial for biological functions of numerous cancer-associated proteins (e.g., RAS, MC1R, PD-L1, GLUT1)[25–28]. For example, ZDHHC9 contributes to glioma progression by promoting the

[1]The Molecular Neuropharmacology Laboratory and the Eye-Brain Research Center, The State Key Laboratory of Eye Health, Wenzhou Medical University, Wenzhou, China. [2]Oujiang Laboratory (Zhejiang Laboratory for Regenerative Medicine, Vision and Brain Health), School of Ophthalmology & Optometry and Eye Hospital, Wenzhou Medical University, Wenzhou, China. [3]These authors contributed equally: Hui Guo, Zhiqing Lin, Di Zhang. ✉e-mail: chenjf555@gmail.com; guoweihaha@wmu.edu.cn

localization of the plasma membrane of GLUT1, leading to high levels of glycolysis[28]. Furthermore, ZDHHC9 can influence the affinity of HRAS and NRAS at the plasma membrane to control tumor development[29]. Furthermore, deletion of ZDHHC9 significantly slowed the progression of acute lymphoblastic leukemia and pancreatic cancer[30,31]. However, it is currently unclear whether palmitoylation plays any role in CD38 regulation at the translational level.

In this study, we describe, for the first time, that CD38 is palmitoylated by ZDHHC9 in position Cys16 and depalmitoylated by APT1. This post-translational modification helps stabilize CD38 in tumor cells. Consequently, a peptide was designed to block CD38 palmitoylation and deplete CD38 expression in cancer cells, and thus inhibiting Pano2 tumor progression. These findings provide additional information on CD38 homeostasis and are helpful for developing new therapeutic strategies targeting CD38 palmitoylation for cancer treatment.

Results

Palmitoylation was responsible for the expression of the CD38 protein in tumor cells

The transcriptional regulation and functional significance of *Cd38* have been studied extensively[15,19,20]. However, how the CD38 protein is regulated by post-translational modifications remains largely elusive. Interestingly, through mass spectrometry studies using the SwissPalm database (https://swisspalm.org/), CD38 was identified as a potential target for palmitoylation modification, a powerful lipid modification that regulates cellular localization and precise protein interaction of numerous membrane-bound proteins[32–34]. To investigate whether CD38 can be modified by palmitoylation, we first used 2-bromopalmitate (2-BP), a typical broad spectrum palmitoyl transferase inhibitor[22], to investigate whether it had an effect on CD38 protein expression in different tumor cells (e.g., Pano2 pancreatic cancer, KPC pancreatic cancer, and LLC Lewis lung carcinoma). We observed a significant decrease in CD38 protein levels in tumor cells after a 24 h treatment with 2-BP (Fig. 1A and Supplementary Fig. 1; Supplementary Data 1). In contrast, CD38 expression was significantly increased when Pano2 cells, KPC cells, and LLC cells were treated with different doses of palmostatin B, a beta-lactone molecule that inhibits all known depalmitoylases, including acyl protein thioesterase 1 (APT1) and 2 (APT2)[35] (Fig. 1B).

Furthermore, treatment of Pano2 cells with 2-BP or palmostatin B, respectively, reduced or increased the expression of CD38 protein in a time-dependent manner (Fig. 1C). Consistently, the effect of 2-BP, palmostatin B and ML348 on the expression of the CD38 protein was also verified by immunofluorescence staining, which was consistent with the results of western blotting assays (Fig. 1D, E; Supplementary Data 1). Collectively, these results suggested that CD38 protein levels in various tumor cells are regulated by S-palmitoylation.

To verify whether CD38 is directly regulated by S-palmitoylation, we performed an acyl-biotin exchange (ABE) assay that allows for specific labeling of palmitoyl proteins, a commonly used tool for detecting S-palmitoylation[36]. First, we generated CD38 constructs tagged with hemagglutinin (HA) and transfected them into HEK293T cells. As shown in Fig. 1F, G, we pulled-down exogenous CD38 protein from cell lysates using HA beads and subjected these to the ABE assay. The results again suggested the presence of palmitoylated CD38. Given that protein palmitoylation events are regarded enzymatically reversible modifications, the addition of 2-BP to HEK293T cells significantly inhibited the palmitoylation level of exogenous expressed CD38 (Fig. 1H, I; Supplementary Data 1). To verify whether endogenous CD38 can be palmitoylated, immunoprecipitation of the CD38 protein was performed with anti-CD38 antibody, followed by the ABE assay using the same approach. Endogenous CD38 is also palmitoylated (Fig. 1J, K; Supplementary Data 1). Additionally, as shown in Fig. 1L, M, palmostatin B significantly increased the palmitoylation level of CD38. Taken together, these results revealed that palmitoylation is responsible for the expression of the CD38 protein in tumor cells.

Palmitoylation at Cys 16 inhibited CD38 proteasomal degradation

To further identify potential palmitoylation modification sites for CD38, we used the UniProt Web tool to analyze the alignment of the protein sequence of CD38 homologs in different species[37] and identified that the amino acid sequence of CD38 has a highly conserved cysteine at position 16 across various species (Fig. 2A). Furthermore, the highly predicted palmitoylation site at Cys16 in human and mouse sequences was also obtained from the CSS-palm 4.0 web tool (Supplementary Fig. 2A)[38,39]. Furthermore, as shown in Fig. 2B, C, CD38 consists of a short N-terminal cytoplasmic domain, a transmembrane domain, and a longer extracellular C-terminal. The location of CD38 site 16 is similar to the palmitoylation site of a typical membrane protein. Based on the above analysis, we hypothesized that cysteine residue 16 of CD38 is a potential palmitoylation site. To determine the palmitoylation site of CD38, a CD38 C16S mutant with HA-tag at the C-terminus was constructed by site-specific mutagenesis at Cys16, the highly predicted palmitoylation site. The wild-type CD38 and CD38 C16S plasmids were then transfected into HEK293T cells, respectively, followed by ABE assays to detect changes in palmitoylation levels. Notably, CD38 palmitoylation levels were significantly reduced compared to controls after mutating cysteine to serine at position 16 (Fig. 2D; Supplementary Data 1). Additionally, to better define the modification site of human CD38 containing an additional cysteine residue at position 15, we mutated the cysteine and assessed its impact on CD38 palmitoylation. The results showed that the C15S mutation did not affect the palmitoylation levels of CD38 (Supplementary Fig. 2B). Palmitoylation modification has been reported to be essential for membrane localization of a large number of membrane-associated proteins[40], thus exogenous EGFP-CD38 and EGFP-CD38-C16S plasmids were introduced into cells to detect subcellular CD38 localization. The results showed that the C16S mutation led to a reduced expression of CD38 on the plasma membrane, while significantly increasing its co-localization with GM130 (a marker for the Golgi apparatus) (Supplementary Fig. 2C). Together, these results revealed that the Cys16 (C16) is the major CD38 N-terminal palmitoylation site.

We then investigated whether palmitoylation modifies CD38 expression in tumor cells by affecting the stability of the CD38 protein. Compared with DMSO treatment, 2-BP treatment accelerated the CD38 turnover rate and promoted CD38 degradation (Fig. 2E). Furthermore, to further confirm the results, we next examined the expression of CD38 in five common tumor cell types (e.g., 4T1, Pano2, LLC, B16F10, and MC38), with the lowest expression levels of CD38 in B16F10 cells (Supplementary Fig. 3). We then used lentiviruses to engineer B16F10 cells to stably express wild-type HA-CD38 and C16S mutations, respectively. The expression of CD38 was observed at different times after adding cycloheximide (CHX). The results of the CHX-chase assay showed that the C16S mutation significantly reduced the stability of the CD38 protein and accelerated protein degradation (Fig. 2F, H). Palmitoylation can affect the protein degradation process and therefore regulate the stability of protein[23]. Next, we asked whether palmitoylation of CD38 affected its stability by influencing the ubiquitin proteasome pathway. Interestingly, treatment with the proteasome inhibitor MG132 almost rescued C16S mutation-mediated downregulation of CD38 protein levels, suggesting that palmitoylation can prevent the degradation of CD38 protein through the proteasome pathway (Fig. 2G, I). Additionally, the level of CD38 ubiquitination increased significantly in cells with C16S mutations compared with that in CD38-WT cells (Fig. 2J). Collectively, these results suggest that CD38 palmitoylation is required for the stability of the CD38 protein and inhibits CD38 degradation through the ubiquitin-proteasome pathway.

ZDHHC9 mediated CD38 palmitoylation and stabilized protein levels in tumor cells

Twenty-three members of the palmitoyl transferase family have been described in mammals. Considering the distribution of CD38 (dominantly in the plasma membrane and only a small number localizing to the cytoplasm)[9] and the general spatial colocalization (substrates and its corresponding palmitoyl transferases), we excluded nine palmitoyl transferases

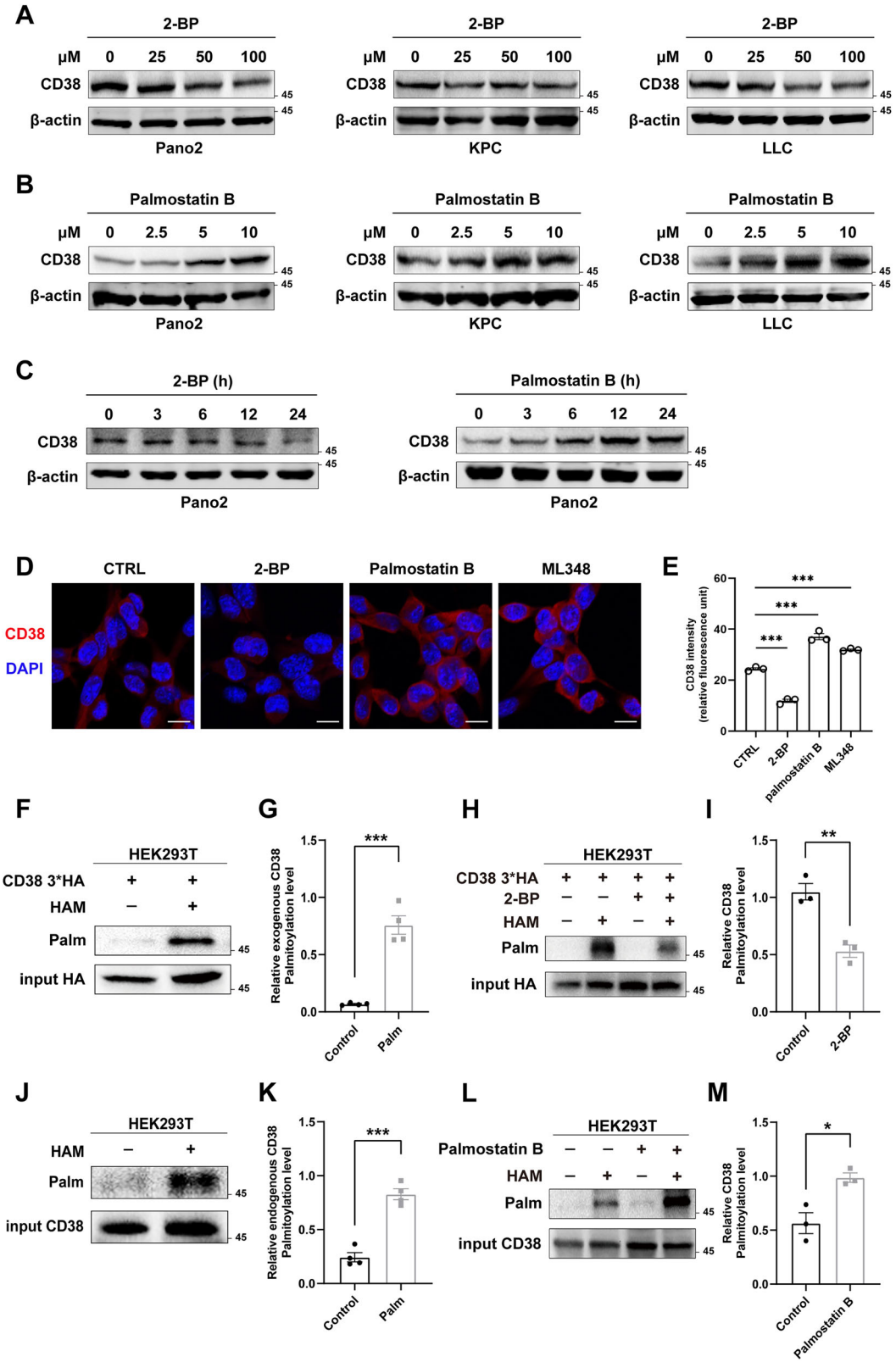

that localized within the nucleus of the cells based on the Human Protein Atlas and literature research[27]. Previous studies have reported the distribution of ZDHHC4 and ZDHHC6 in the ER[41,42], ZDHHC20 at the ER[43] and plasma membrane[44], however, our data showed that the expression of CD38 protein and its palmitoylation level did not alter after transfecting HEK293T cells with plasmids encoding HA-tagged ZDHHC4, ZDHHC6, and ZDHHC20 at different concentrations (Supplementary Fig. 4D and E). Thus, we next expanded our analysis to the remaining enzymes, including ZDHHC2, ZDHHC3, ZDHHC5, ZDHHC7, ZDHHC9, ZDHHC11, ZDHHC13, ZDHHC14, ZDHHC17, ZDHHC18, and ZDHHC21. The siRNA sequences were selected according to the previous literature[27]. To this aim, the aforementioned enzymes were silenced separately using siRNA

Fig. 1 | CD38 palmitoylation dynamically modulates the protein expression of CD38. A, **B** Pano2, KPC, and LLC cells were incubated with indicated concentrations of 2-BP (**A**) and palmostatin B (**B**) for 24 h and expression of CD38 was evaluated by western blotting analysis. **C** Western blotting showing the protein expression of CD38 in Pano2 cells treated with 2-BP (100 μM) and palmostatin B (10 μM) at the indicated time points. **D** Immunofluorescence assay detecting CD38 expression in Pano2 cells treated with 100 μM 2-BP, 10 μM palmostatin B, and 10 μM ML348 for 24 h. CD38 is stained red and the cell nucleus is stained with 4′,6-diamidino-2-phenylindole (DAPI) and appears blue. Scale bars, 10 μm. **E** Quantification of the intensity of the immunofluorescence of CD38 using ImageJ software. **F** Exogenous CD38 palmitoylation was detected in HEK293T cells using ABE assay and quantification (**G**). **H** Analysis of the ABE assay showing the level of CD38 palmitoylation in HEK293T cells with or without 2-BP (100 μM) treatment and quantification (**I**). **J** Palmitoylation of endogenous CD38 in HEK293T cells was detected using ABE assay and quantification (**K**). **L** ABE assay analysis demonstrated that the palmitoylation level of CD38 increased following treatment with palmostatin B and quantification (**M**). All results are presented as mean ± SEM. **E** Statistical analyses were calculated using a one-way ANOVA with a Tukey post hoc test ($n = 3$). **G**, **I**, **K**, **M** Statistical analyses were calculated using unpaired Student's t-test ($n = 3$ or 4) (ns not significant, $^{*}p < 0.05$, $^{**}p < 0.01$, and $^{***}p < 0.001$).

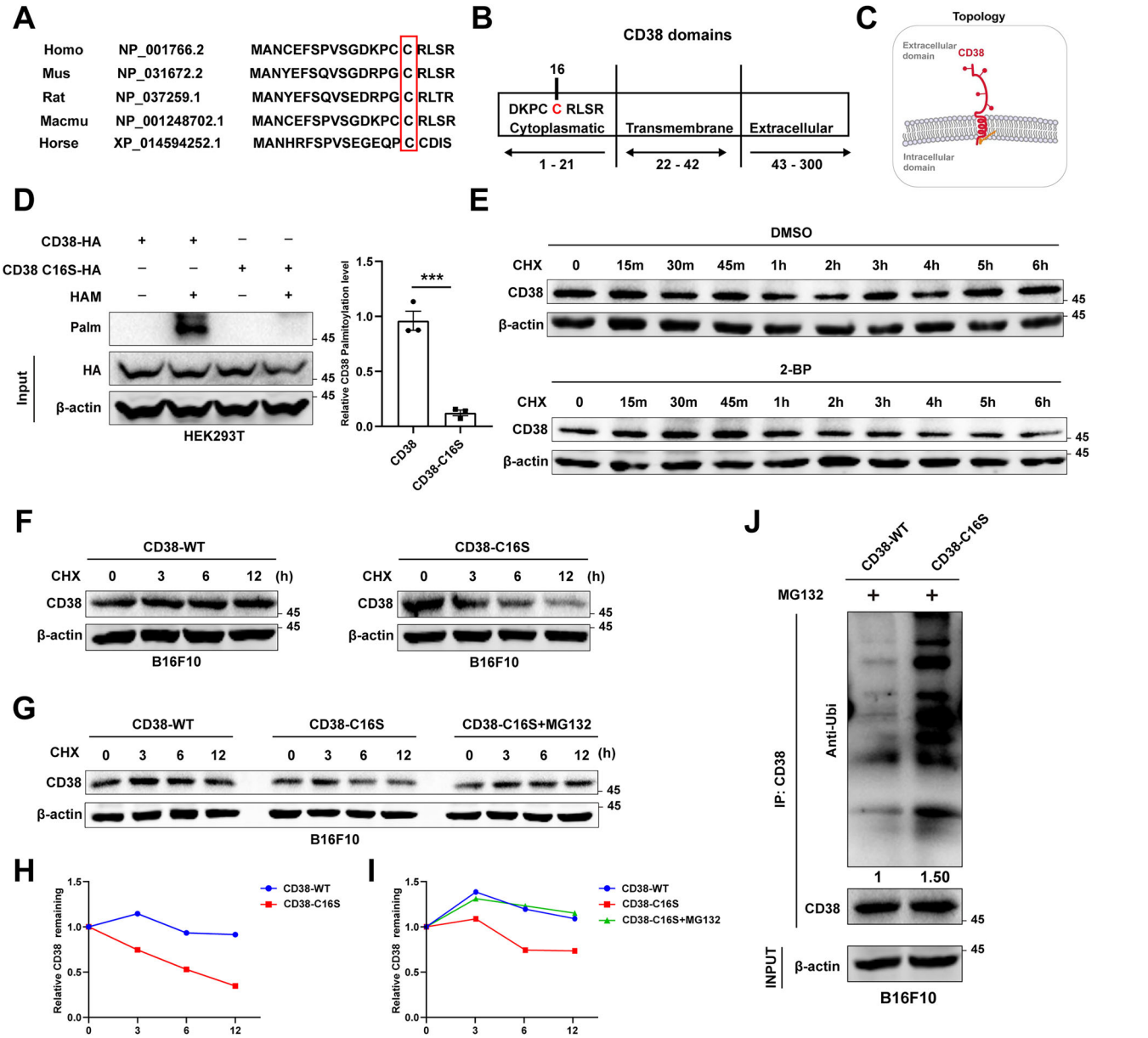

Fig. 2 | CD38 is palmitoylated at Cys16. A Sequences of amino acids of CD38 in various species showing conserved cysteine at position 16. **B** Schematic diagram of the structure of the CD38 molecule. The CD38 domains contained intracellular (20 amino acids), transmembrane (23 amino acids), and extracellular (257 amino acids). **C** Topology model of CD38 palmitoylation. **D** Western blotting analysis showing the level of S-palmitoylation of CD38 WT and C16S in HEK293T cells. **E** Western blotting analysis showing decreased expression of the CD38 protein in Pano2 cells treated with 2-BP and CHX at the indicated time compared to DMSO treatment. **F** Western blotting analysis of CD38 stability in CHX pretreated CD38-WT and CD38-C16S B16F10 cells and qualification (**H**) and (**G**). The CD38-C16S B16F10 cells were treated with MG132 and the western blotting assay was used to detect CD38 protein levels and qualification (**I**). **J** CD38 ubiquitination assay in B16F10 cells. The CD38-WT and CD38-C16S mutant cells were treated with MG132 followed by the western blotting assay to detect CD38 and ubiquitin. All results are presented as mean ± SEM. **D** Statistical analyses were calculated using unpaired Student's t-test ($n = 3$) (ns not significant, $^{*}p < 0.05$, $^{**}p < 0.01$, and $^{***}p < 0.001$).

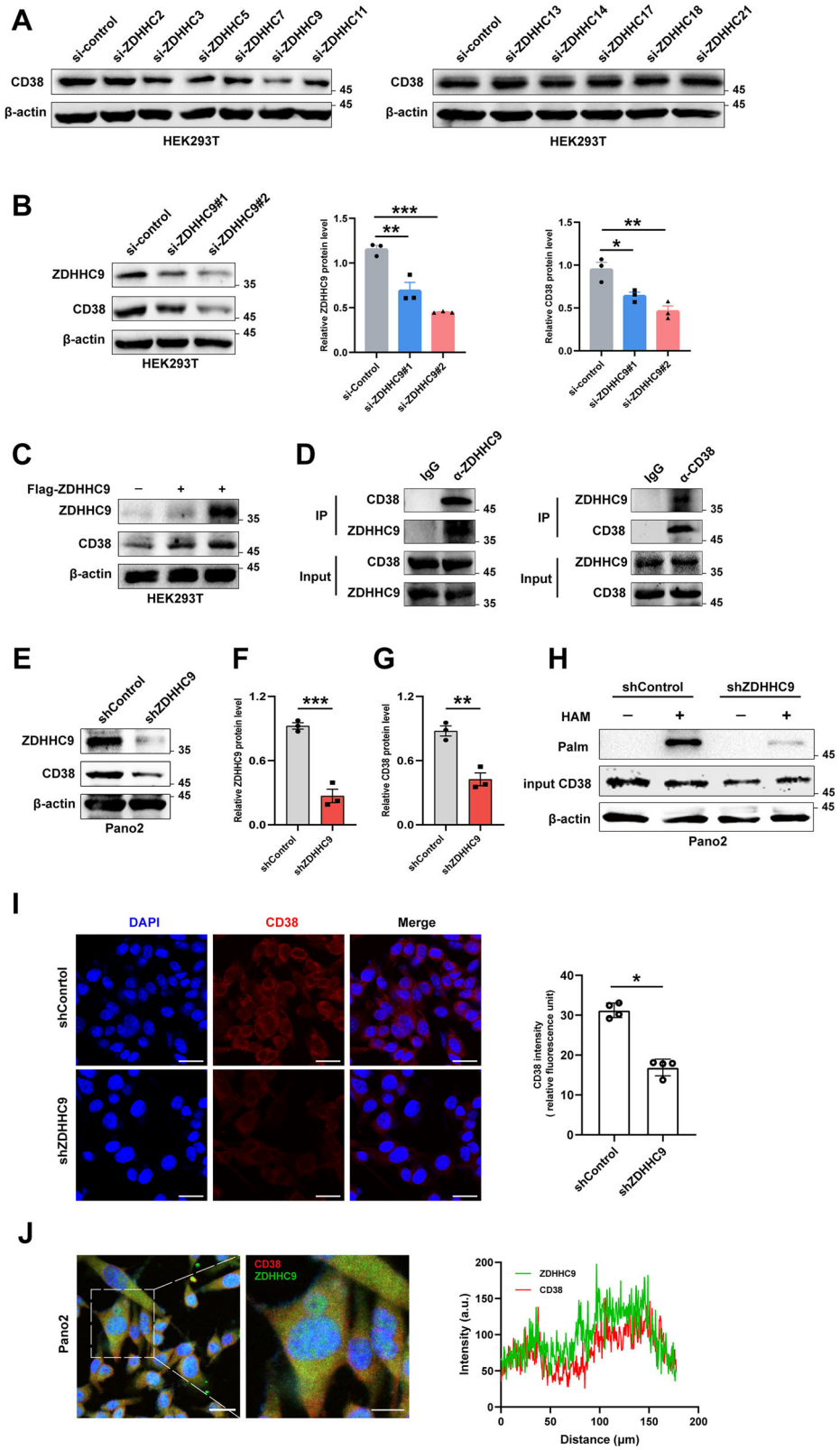

Fig. 3 | CD38 is palmitoylated by ZDHHC9. **A** Western blotting analysis showing the expression of CD38 after transfected with different siRNA from ZDHHC enzymes in HEK293T cells. **B** Western blotting assay detecting the protein level of CD38 in HEK293T cells that were transfected with two independent siRNAs targeting ZDHHC9 and quantification. **C** Expression of CD38 in HEK293T cells transfected with different concentration flag-tagged ZDHHC9 vector. **D** A reciprocal co-IP assay was performed to detect the interaction between endogenously expressed ZDHHC9 and CD38 in HEK293T cells. **E** Western blotting was used to detect the endogenous expression of the CD38 protein in Pano2 cells with ZDHHC9 stably knocked down. **F** Quantification of ZDHHC9 protein levels. **G** Quantification of CD38 protein levels. **H** Endogenous CD38 protein was immunoprecipitated from ZDHHC9 knockdown cells and subjected for ABE analysis. **I** Left, representative immunofluorescence images of CD38 staining (red) of shZDHHC9 cells and shControl cells (blue, DAPI-labelled cell nuclei). (Scale bars, 20 μm). Right, corresponding quantification analysis. **J** Immunofluorescence assay showing the colocalization of CD38 and ZDHHC9 in Pano2 cells and statistical analysis. (Scale bars, 50 μm). All results are presented as mean ± SEM. **B** Statistical analyses were calculated using a one-way ANOVA with a Tukey post hoc test ($n = 3$). **F**, **G**, **I** Statistical analyses were calculated using unpaired Student's t-test ($n = 3$ or 4) (ns not significant, $^{*}p < 0.05$, $^{**}p < 0.01$, and $^{***}p < 0.001$).

targeting technology. In particular, the results of western blotting showed marked suppression of CD38 protein levels when ZDHHC9 was knocked down in HEK293T cells (Fig. 3A). To confirm that this phenomenon was not caused by potential off-target effects of siRNA, two independent, non-overlapping siRNA sequences were employed. Consistently, silencing of ZDHHC9 with an additional independent siRNA (siZDHHC9#2) also significantly reduced CD38 protein levels (Fig. 3B; Supplementary Data 1). Next, when we transfected HEK293T cells with increasing amounts of the flag-tagged ZDHHC9 protein plasmid, we found that the concentration of the CD38 protein increased considerably with increasing expression of ZDHHC9 (Fig. 3C). Furthermore, since palmitoyl transferases have previously been shown to interact with certain substrates, we hypothesized that

ZDHHC9 mediates CD38 palmitoylation by directly interacting with CD38. As expected, co-immunoprecipitation (Co-IP) assays indicated that endogenous ZDHHC9 indeed interacted with CD38 (Fig. 3D).

To further validate our findings, we used the lentivirus-mediated shRNA approach to silence endogenous expression of ZDHHC9 in Pano2 tumor cells. Quantitative polymerase chain reaction (QPCR) and western blotting results confirmed a successful knockdown of ZDHHC9 (Fig. 3F and Supplementary Fig. 4A; Supplementary Data 1). It should be noted that ZDHHC9 knockdown only attenuated the level of CD38 protein levels, while this did not occur at the level of mRNA (Fig. 3E, G and Supplementary Fig. 4B; Supplementary Data 1), suggesting that ZDHHC9 regulation in CD38 protein levels was at the post-translational level. Furthermore, the ABE assay confirmed that CD38 palmitoylation levels were markedly decreased when ZDHHC9 knocked down compared to the control group (Fig. 3H). Consistently, ABE analysis showed that ectopic expression of the catalytically inactive DHHC9 mutant (DHHC9-C169S) significantly reduced CD38 palmitoylation levels compared to the wild-type DHHC9 (DHHC9-WT) (Supplementary Fig. 4C). Meanwhile, an immunofluorescence assay revealed that CD38 levels were downregulated in ZDHHC9-knockdown tumor cells (Fig. 3I; Supplementary Data 1). In addition, there was subcellular colocalization of endogenously expressed ZDHHC9 and CD38 in Pano2 cells (Fig. 3J). Next, we speculated that ZDHHC9-mediated CD38 palmitoylation can stabilize its expression in tumor cells. We quantified intracellular CD38 protein levels after pretreatment of ZDHHC9 knockdown and control Pano2 cells with CHX for 0, 3, 6, and 12 h, respectively. The results showed that the CD38 degradation rate in Pano2 cells increased significantly after inhibition of ZDHHC9 expression (Supplementary Fig. 4F). Thus, these results suggest that ZDHHC9 is a major enzyme for palmitoylation of CD38, which maintains high levels of CD38 expression in tumor cells by affecting its protein stability.

CD38 is depalmitoylated by APT1

To further identify the enzymes catalyzing the depalmitoylation of CD38, we used ML348 and ML349, two validated pharmacological tools to inhibit APT1 and APT2 activity in mammalian cells[45], respectively. After a 24 h treatment in tumor cells, we observed that treatment with ML348 rather than ML349 increased the expression of CD38 protein (Fig. 4A). Next, we used small interfering RNA (siRNA) to knock down APT1 and APT2 individually. The results showed that CD38 expression increased upon APT1 knockdown, whereas no significant changes were observed with APT2 knockdown (Fig. 4B–D and Supplementary Fig. 5A–C; Supplementary Data 1). Consistently, when HA-tagged APT1 and APT2 were overexpressed in HEK293T cells, the results showed that APT1 overexpression decreased CD38 protein levels, whereas APT2 overexpression had no effect on CD38 protein expression (Fig. 4E–G and Supplementary Fig. 5D–F; Supplementary Data 1). Furthermore, Co-IP assays confirmed the interaction of CD38 with APT1 (Fig. 4H). We also examined whether co-expressing APT1 and CD38 plasmids in cells could downregulate the palmitoylation level of CD38. Indeed, the results revealed that the co-expressing of APT1 with CD38 significantly diminished the palmitoylation level of CD38 (Fig. 4I). Together, the above data suggested that APT1 is the primary acylprotein thioesterase for CD38.

A peptide was designed that inhibited CD38 palmitoylation by blocking ZDHHC9 and CD38 interaction

We designed a competitive peptide that could interfere with the interaction between ZDHHC9 and CD38 to specifically inhibit CD38 palmitoylation. We first designed an experimental peptide containing a CD38 palmitoylation site at Cys16 and a control peptide with a mutant palmitoylation site. Furthermore, to improve the intracellular transport efficiency of the peptide, we fused the cell penetrating peptide (CPP) to the experimental peptide (CPPtat-S1) and the control peptide (CPPtat-S1 control) (Fig. 5A). Next, we used the ABE method to detect CD38 palmitoylation after co-incubating the different peptides with the cells. Obviously, the CPPtat-S1 peptide, but not the CPPtat-S1 control peptide, significantly attenuated CD38 palmitoylation (Fig. 5B). Furthermore, we noted that the control peptide of CPPtat-S1 did not influence CD38 expression, whereas CD38 expression decreased dose-dependently after treatment with the CPPtat-S1 peptide (Fig. 5C, D; Supplementary Data 1). Interestingly, the CPPtat-S1 peptide only altered the levels of the CD38 protein, without affecting its transcriptional activity (Fig. 5E; Supplementary Data 1). Similarly, the same effect was also observed in LLC cells (Supplementary Fig. 6A–C). Additionally, the CPPtat-S1 peptide dramatically inhibited pancreatic cancer cell growth and migration (Fig. 5F–H; Supplementary Data 1). Given that the human and mouse CD38 C16 sites encode different amino acid sequences, we further designed a competitive peptide that targeted the palmitoylation motif of human CD38: CPPtat-S2 (Supplementary Fig. 6D). Next, we evaluated the effect of CPPtat-S2 on CD38 expression in MIAPaCa-2 cells from human pancreatic cancer, a cell line with high expression of CD38. We observed a similar effect that the CPPtat-S2 peptide targeting human CD38 sequences inhibited the expression of the CD38 protein (Supplementary Fig. 6E).

Intratumoral injection of a peptide that inhibits CD38 palmitoylation suppressed tumor progression

To further validate the oncogenic role of CD38 in pancreatic cancer, we constructed a tumor model using Pano2 cells with stable CD38 knockdown. We confirmed the knockdown efficiency of CD38 at the transcriptional and protein levels using QPCR, western blotting, and flow cytometry analysis (Supplementary Fig. 7A–D). Next, we select stable clones with the highest CD38 knockdown efficiency for the follow-up study. CCK-8 and colony formation assays were used to assess tumor cell proliferation ability in vitro. As shown in Supplementary Fig. 7E, F, the knockdown of CD38 expression in Pano2 cells showed a significant decrease in proliferation compared with the control group. Next, to assess tumor growth in vivo, shControl or shCD38 Pano2 cells were subcutaneously inoculated into immunocompetent C57BL/6 mice. The results showed that CD38 knockdown markedly suppressed Pano2 tumor growth in vivo (Supplementary Fig. 7G, H), indicating that CD38 expression could facilitate the malignant progression of Pano2 pancreatic carcinoma. Next, we validated whether specific inhibition of palmitoylation of CD38 by competitive peptides could delay Pano2 tumor growth. First, we established a subcutaneous mouse model of pancreatic cancer (Fig. 6A). Briefly, 5×10^6 Pano2 cells were implanted subcutaneously into the right flank of immunocompetent C57BL/6 mice, and then tumor growth was monitored every 2 to 3 days. When the average tumor size increased around 100 mm^3, we randomly divided the mice into three groups: mice treated with Vehicle, CPPtat-S1 Control peptide, and CPPtat-S1 peptide, respectively. The CPPtat-S1 peptide was injected intratumorally into Pano2 tumor-bearing mice every 2 days. Finally, tumors were harvested 2 days after the last treatment. In particular, we observed that Pano2 tumors treated with CPPtat-S1 grew significantly slower in terms of tumor size and tumor weight compared to controls (Fig. 6B–D; Supplementary Data 1). Immunohistochemical (IHC) staining showed that the total number of Ki67 cells decreased after treatment with CPPtat-S1, whereas the number of apoptotic cells did not change significantly (Fig. 6E–G; Supplementary Data 1). Additionally, peptide treatment did not cause any loss of body weight in mice compared with the starting body weight in any of the animals (Supplementary Fig. 8). Collectively, these results suggested that the prepared CPPtat-S1 peptide could effectively inhibit Pano2 tumor progression by inhibiting palmitoylation of CD38.

Discussion

In this study, we demonstrate a crucial role for palmitoylation in regulating the stability of the CD38 protein. The effects of targeting CD38 palmitoylation using a specific peptide on CD38 expression revealed modulation of this post-translational modification as a promising therapeutic strategy against cancer development.

Previous studies have focused predominantly on the role of CD38 in hematological malignancies, while the effects of CD38 expression on multiple types of solid tumors receives growing research attention[6,7,46,47]. These findings have characterized the functional role of CD38 in solid tumors

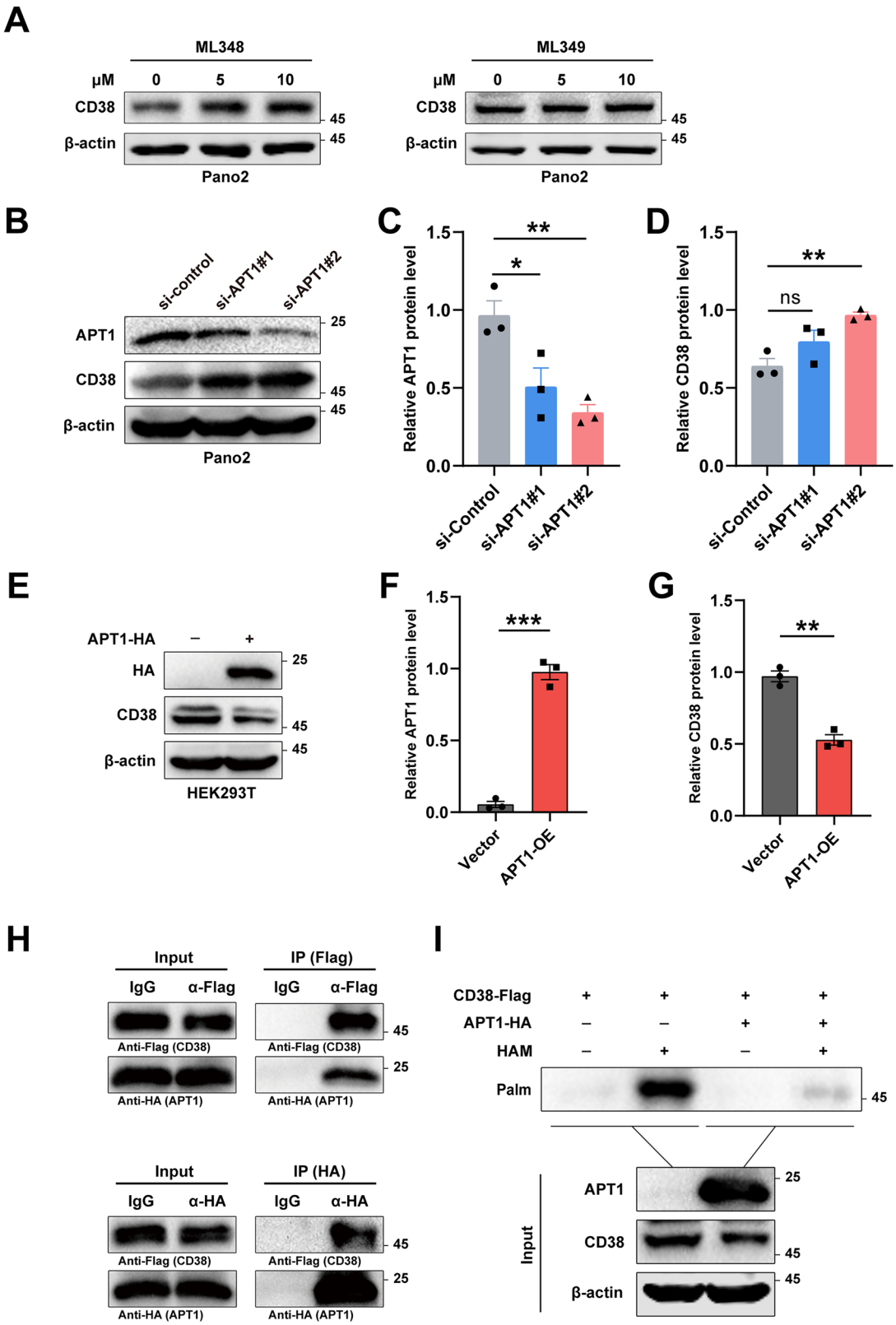

Fig. 4 | APT1 is the primary acylprotein thioesterase for CD38. A Pano2 cells were incubated with indicated concentrations of ML348 and ML349 for 24 h and the expression of CD38 was evaluated by western blotting analysis. **B** Western blotting assay detecting the protein level of CD38 in Pano2 cells that were transfected with two independent siRNAs targeting APT1 and quantification (**C**) and (**D**). **E** Expression of CD38 in HEK293T cells overexpressing APT1 and quantification (**F**) and (**G**). **H** Co-IP analysis of the interaction of CD38 and APT1 in HEK293T cells. **I** CD38 palmitoylation in HEK293T cells with ectopic expression of APT1 detected by ABE assay. All results are presented as mean ± SEM. **C**, **D** Statistical analyses were calculated using a one-way ANOVA with a Tukey post hoc test ($n = 3$). **F**, **G** Statistical analyses were calculated using unpaired Student's t-test ($n = 3$) (ns not significant, $^{*}p < 0.05$, $^{**}p < 0.01$, and $^{***}p < 0.001$).

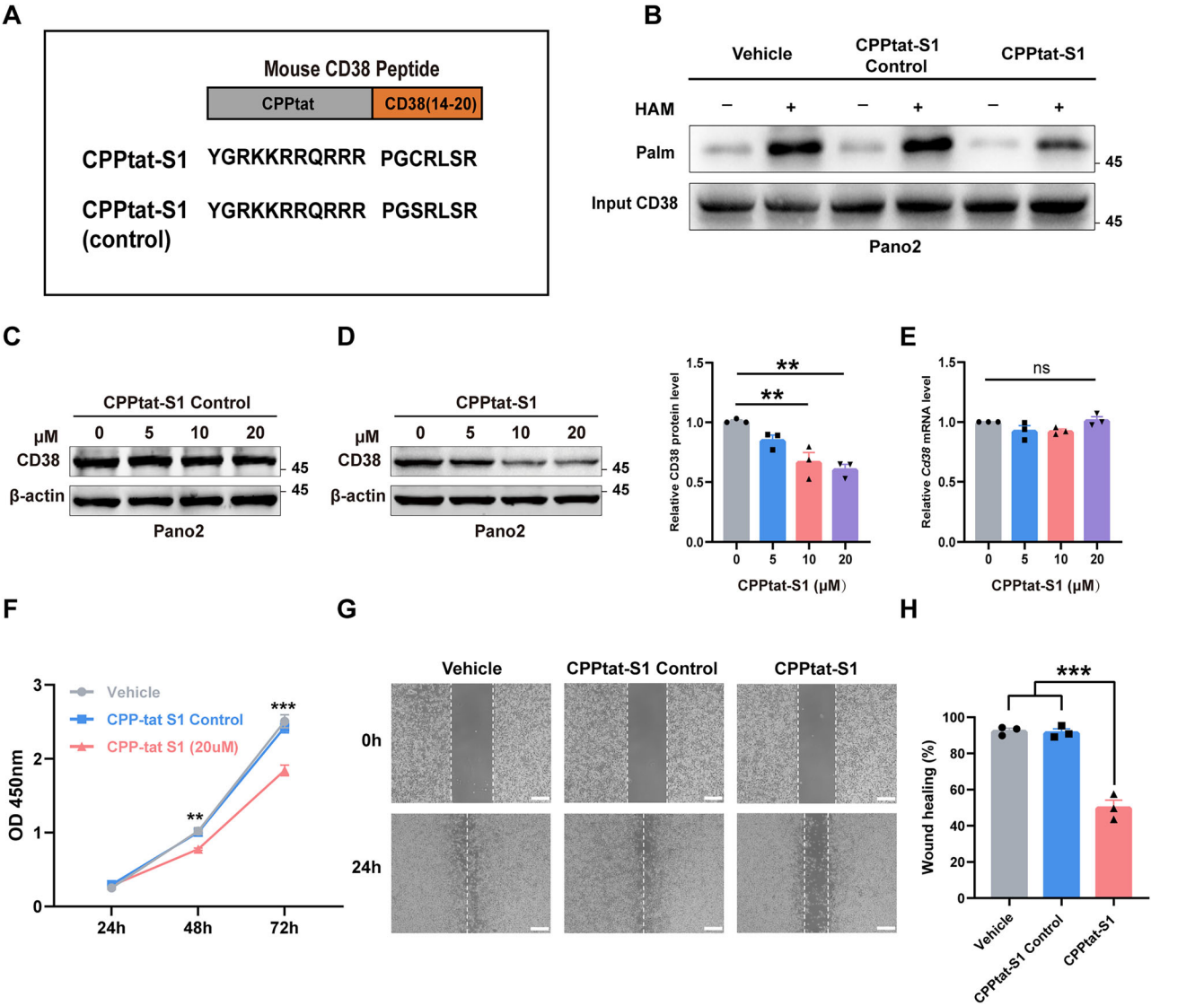

Fig. 5 | A peptide designed to inhibit CD38 palmitoylation and protein expression. A Sequence diagram of mouse CD38 peptide. **B** Pano2 cells were treated with CPPtat-S1 Control peptide or the CPPtat-S1 peptide and subjected to the ABE assay. **C** Western blot analysis showing the effect of CPPtat-S1 Control peptide incubation on CD38 protein expression in Pano2 cells. **D** Pano2 cells were treated with CPPtat-S1 peptide and subjected to western blotting assay and quantification analysis. **E** The mRNA level of *Cd38* analyzed by qPCR after CPPtat-S1 peptide treatment. **F** Pano2 cells were pretreated with peptide, then cell viability was analyzed using the CCK8 cell proliferation assay. **G** The effect of peptide treatment on Pano2 cell migration was detected by the scratch test and quantification (**H**). (Scale bars, 100 μm). All results are presented as mean ± SEM. **D**–**H** Statistical analyses were calculated using a one-way ANOVA with a Tukey post hoc test ($n = 3$) (ns not significant, $^{**}p < 0.01$, and $^{***}p < 0.001$).

based on abnormal high expression of CD38 in a wide variety of tumors whose overexpression is correlated with tumor progression, invasion, and metastasis[46]. For example, CD38 was highly expressed in human nasopharyngeal carcinoma cell lines and may play an oncogenic role by affecting energy metabolism[48]. Furthermore, CD38 deficiency substantially attenuated tumor growth and prolonged the life span of glioma-bearing mice[49]. In esophageal cancer, upregulated expression of CD38 was also confirmed in myeloid-derived suppressor cells (MDSCs), and the administration of an anti-CD38 monoclonal antibody suppressed tumor growth[50]. These results demonstrate that regulation of CD38 expression plays a pivotal role in tumor control, with the majority of studies having focused primarily on the transcriptional level. Our identification of the palmitoylation modification of CD38 will provide further insight into the regulatory mechanisms of CD38 in tumor cells.

Currently, CD38-targeting antibodies have been used in the clinical treatment of multiple myeloma[14], exhibiting promising efficacy and safety profiles. However, not all patients respond to monotherapy, and many patients eventually develop resistance over time[51]. CD38 antibodies exert therapeutic effects mainly through Fc-dependent immune effector mechanisms, including antibody-dependent cell-mediated cytotoxicity, complement-dependent cytotoxicity, and antibody-dependent cellular phagocytosis[12]. CD38 expression on MM cells decreases after antibody treatment, but after a period of time, the expression of CD38 returns to its original level[12]. Furthermore, the expression of CD38 is associated with the response to daratumumab monotherapy[51]. In addition, CD38 is distributed not only in the plasma membrane, but also in cytoplasmic organelles such as the nuclear membrane, mitochondria, and endoplasmic reticulum, whereas intracellular CD38 cannot be blocked by antibodies[5]. In the present study, we found that palmitoylation can regulate CD38 expression in the whole cell, and the designed peptide, which specifically inhibited endogenous CD38 palmitoylation and expression on a variety of tumor cells, can significantly delay the tumor progression of Pano2 pancreatic cancer. In this regard, the palmitoylation-based targeting approach, which affects the target protein within the entire cell, may provide more robust and persistent

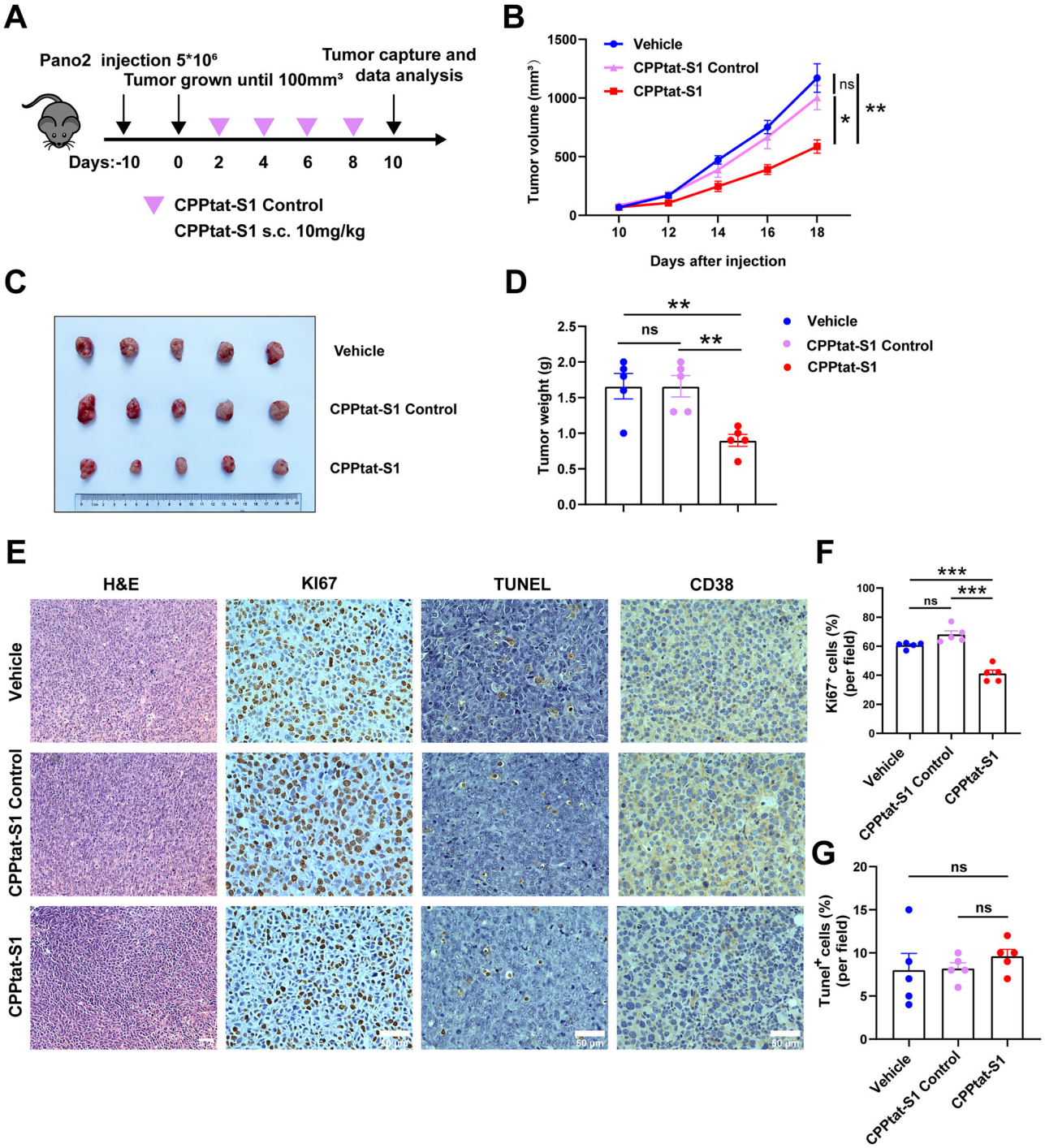

Fig. 6 | Inhibition of CD38 palmitoylation by peptides slows Pano2 pancreatic cancer growth. A–D C57BL/6 mice were subcutaneously injected with Pano2 cells and treated with DMSO (Vehicle group), CPPtat-S1 Control peptide, or CPPtat-S1 peptide (10 mg/kg). **A** Schematic diagram showing the treatment plan. **B–D** Tumor volumes were measured every 2 days. Tumor size was weighed and photographed at the end of treatment. **E** After peptide treatment, a part of the tumor tissue was removed and paraffin embedded, and representative images of HE staining and IHC staining (Ki67, Tunel, CD38) were obtained. The scale is 50 μm. **F, G** The number of positive cells in Ki67 and Tunel under 40× mirror field was quantified by IHC staining. All results are presented as mean ± SEM. **B–G** Statistical analyses were calculated using a one-way ANOVA with a Tukey post hoc test ($n = 5$) (ns not significant, $^{*}p < 0.05$, $^{**}p < 0.01$, and $^{***}p < 0.001$).

suppression effects. The strategy is supported by other available peptides that target palmitoylation of certain proteins. Yao et al. designed a competitive inhibitor of PD-L1 palmitoylation that decreases PD-L1 expression on the cell membrane and in the recycling of endosomes, thus enhancing T-cell immunity against the tumours[27]. Recently, Sun et al. developed a biologically active Proprotein convertase subtilisin/kexin type 9 (PCSK9)-derived peptide that competitively inhibits PCSK9 palmitoylation and increases the antitumor effects of sorafenib in advanced hepatocellular carcinoma[52]. Until now, no inhibitors specific to individual ZDHHC enzymes have been identified[53]. The design of compounds or peptides specifically targeting the palmitoylation site presents an interesting alternative with great potential[54]. Additional studies are required to optimize the pharmacological properties of the CD38-targeting peptide and enhance their stability in vivo.

Our present study revealed the role of palmitoylation-modified upregulated CD38 in cancer development; however, whether such a mechanism

is universal in other physiological processes is an interesting question waiting for further investigation. In the brain, CD38 is involved in inflammation processes and psychiatric disorders[55,56]. CD38 is a major factor involved in aging and its levels increase in several mouse tissues (including liver, white adipose tissue, spleen, and skeletal muscle) with age[2,57]. In a recent study, Zhang et al. reported that CD38 is increased in both the hippocampus and cortex in the lipopolysaccharide-induced depression-like model[58]. Accordingly, the level of palmitoylation of CD38 and the level of ZDHHC9 deserves further study.

Methods

Cell culture and transfection

Mouse Lewis lung carcinoma LLC cells, human colorectal cancer HCT116 cells, mouse pancreatic cancer Pano2 cells, and human pancreatic cancer MIA PaCa-2 cell lines, Mouse Melanoma B16F10 cells, HEK293T cells were purchased from the American Type Culture Collection (ATCC). The KPC cancer cell line derived from (KrasG12D/+; Trp53R172H/+; Pdx1-Cre mice) was obtained from the Model Organisms Center, Inc. (Shanghai, China). All cell lines were tested and verified to be free of Mycoplasma. Pano2 cells were cultured in RPMI 1640 medium containing 10% fetal bovine serum (FBS, Excellbio) and 1% penicillin/streptomycin (P/S, Beyotime). LLC, MIA PaCa-2, HCT116, KPC, B16F10, HEK293T cells were grown in Dulbecco's Modified Eagle Medium (DMEM) with 10% fetal bovine serum and 1% penicillin/streptomycin. All cells were incubated in an incubator with 5% CO2 at 37 °C.

For the transfection assay, plasmids were purchased from Tsingke Biological Technology (Wuhan, China). First, cells were planted in culture plates and transfection began when the cell density reached 50–60%. Next, 2 μg of plasmids (Tsingke, China) and 4 μL of transfection reagent (Tsingke, China) were mixed with 250 μL Opti-MEM (Gibco, USA), respectively. The plasmid mixture and the transfection reagent mixture were mixed and incubated at room temperature for 20 min, and finally the complex was added to the cells for 6 h. After transfection, the medium was changed to complete normal medium for an additional 48 h.

Western blotting analysis

Cells were lysed with RIPA buffer (Beyotime, China) containing 1% protease inhibitor (Bimake, USA) and 1% phosphatase inhibitor (Bimake, USA) on ice for 10 min after cells were washed with PBS. The cell lysate was then centrifuged at 12,000 rpm for 10 min at 4 °C, the supernatants were used to test protein concentration using the BCA Protein Assay Kit (Beyotime, China). After the protein concentration was determined, 5× SDS-PAGE loading buffer (Beyotime, China) was added to the cell lysate and then the mixture was boiled at 95 °C or 8 min. Next, equal protein samples were separated using SDS-PAGE gel and transferred to nitrocellulose filter membranes (HATF00010, Millipore). The membranes were then placed on a shaker and blocked with 1% BSA for 1 h 30 min at room temperature. After the blocking time, the membranes were incubated with primary antibodies including CD38 (60006-1-Ig, 1:1000, Proteintech), CD38 (ab108403, 1:500, Abcam), ZDHHC9 (HPA031814, 1:500, Millipore), ZDHHC9 (24046-1-AP, 1:500, Proteintech), APT1 (ab91606, 1:5000, Abcam), APT2 (sc-390546, 1:200, Santa Cruz Biotechnology), HA-Tag (3724S, 1:1000, Cell Signaling Technology), DYKDDDDK-Tag(14793S, 1:1000, Cell Signaling Technology), β-actin (20536-1-AP, 1: 20,000, Proteintech) overnight at 4°C. The next day, the corresponding secondary antibodies were added to the membranes for 1 h 30 min at room temperature. Lastly, the membrane protein bands were visualized using ECL reagent and ChemiDoc XRS + imager (Bio-Rad Laboratories Inc., USA).

Immunofluorescence staining

Microscope slides were pre-placed in a cell culture plate and the cells were seeded onto the slides. When the appropriate confluency was reached, the culture medium was aspirated and the cells were washed with cold sterile PBS before being fixed with 4% paraformaldehyde (PFA) for 15 min at room temperature. The slides were washed with PBS for 5 min three times. Cells were blocked in blocking solution (2% BSA (Beyotime, China) and 0.5% TritonX-100 (Beyotime, China) for 1 h at room temperature, and incubated with the primary antibodies against CD38 (60006-1-Ig, 1:1000, Proteintech), ZDHHC9 (24046-1-AP, 1:500, Proteintech) overnight at 4 °C. Subsequently, the cells were rewarmed for 30 min, followed by washing with cold PBS for 5 min three times. After washing, the cells were treated with secondary antibodies in a light shield box for 1 h at room temperature. Finally, cell nuclei were stained with antifade mounting medium with DAPI (Beyotime, China) for 5 min. Images were acquired with a Leica DM6B microscope or a Zeiss LSM 880 NLO confocal microscope.

Quantitative real-time PCR

Total RNA was extracted from cells using the RNAprep Pure Micro Kit (TIANGEN Technology, China), according to the supplier's recommendations. NanoDrop 2000 (Thermo Fisher Scientific) was used to measure RNA concentration and quality. The cDNA was then acquired with a HiScript III RT SuperMix for qPCR (+gDNA wiper) (Vazyme, China), according to the manufacturer's instructions. Briefly, the first step was to further remove genomic DNA from RNA and then prepare the reverse transcriptional reaction system for reverse transcription. The reaction mixture was a total of 20 μL. The relative levels of mRNA expression were determined using an ABI QuantStudio 3 system (ABI, CA, USA). The following thermal cycling program was used: 3 min at 95 °C, 40 cycles of a two-step PCR, 95 °C for 10 s followed by 55 °C for 30 s, and a final extension from 65 to 95 °C for 5 s. Finally, the results were calculated using the $2^{-\Delta\Delta Ct}$ method with GAPDH as an internal reference.

Cell proliferation assay

Cells were digested with 0.25% trypsin (New Cell and Molecular Biotech, Suzhou, China) and seeded at a density of 2000 cells in 100 μL medium per well in 96-well plates. According to the indicated time points shown, the growth medium was discarded, washed three times with PBS, and then 100 μL fresh medium containing 10 μL of Cell Counting Kit-8 (CCK-8) (Dojindo, Kumamoto, Japan) was added to each well. The 96-well plates were cultured in an incubator with 5% CO_2 at 37 °C for 2 h with protection from light. The optical density (OD) was measured at the wavelength of 450 nm using the Spectra Max M5 microplate reader (Molecular Devices, Sunnyvale, CA, USA).

Wound scratch assay

The wound scratch assay was carried out using the μ-dish (IBIDI, Germany), following the manufacturer's instructions. Briefly, the μ-dish was placed into the 6-well plates in advance. Cells were digested with 0.25% trypsin and seeded at a concentration of 2×10^5 cells per well in serum-free medium. When the cells almost covered the bottom of the plates, the μ-dish were carefully removed, the old medium discarded and washed with PBS twice. The cells were then incubated in serum-free medium with corresponding drugs at 37 °C and 5% CO_2 for 0 h and 24 h. Photographs of each well were obtained using an inverted microscope (Leica DMi8, Wetzlar, Germany). Image J software was used to evaluate the extent of cell migration.

Colony formation assay

Briefly, Pano2 shControl cells and shCD38 cells were digested with 0.25% trypsin and these cells were counted using a cell counter plate, respectively. The cells were then seeded in 6-well plates (500 cells per well) and incubated in normal medium with 2 μL/mL puromycin. The medium was changed every two days. After 14 days, cells were fixed with 4% PFA for 30 min at room temperature and stained with 1% crystal violet solution (Sangon Biotech, China) for 20 min. The corresponding cell culture wells were photographed with a camera and then the images were manipulated using adobe illustrator (v.2020).

Flow cytometry

Pano2 shControl cells and shCD38 cells were seeded at 2×10^5 cells per well in a 12-well plate and cultured overnight. Cells were digested with 0.25% trypsin and centrifuged at 1000 rpm for 4 min. 4% PFA was added to fix the cells for 15 min. Then, the cells were washed three times with PBS and centrifuged at 2000 rpm for 4 min. Cells were blocked in blocking solution for 1 h and incubated with the PE-CY7 conjugated CD38 antibody diluent on the ice. After being washed three times with PBS, the cell signal was analyzed using a BD C6 plus flow cytometer. Data analysis was performed using FlowJo software.

Immunohistochemistry

At the end of treatment, the mice were euthanized. Tumors were harvested and fixed with 4% PFA. Subsequently, the tumors were embedded in paraffin and then cut into paraffin sections at a thickness of 5 μm. The paraffin sections were deparaffinized in xylene and rehydrated in a graded ethanol series. The sections were washed with distilled water for 5 min three times. The slices were then boiled in sodium citrate buffer to restore the antigen. The slices were removed and cooled to room temperature, followed by washing with PBS for 5 min three times. Next, quenching the activity of endogenous peroxidase with a 3% hydrogen peroxide for 15 min at room temperature. After washing with PBS, the sections were blocked in blocking buffer (3% BSA) for 30 min. Gently shaken from the blocking buffer, the sections were incubated with primary antibodies and placed flat in a wet box at 4 °C overnight. The next day, the sections were incubated with biotin-labeled secondary antibodies for 2 h and subjected to incubation with HRP (horse radish peroxidase)-labeled streptavidin for 1 h. The signal detection was then performed using the DAB reagent kit (Servicebio, Wuhan), according to the supplier's recommendations. Lastly, the slides were imaged using a Leica DM6B microscope or a Zeiss LSM 880 NLO confocal microscope.

Mice xenograft model

C57BL/6 mice (6-8 weeks old, male) were purchased from Beijing Vital River Laboratory Animal Technology Co., Ltd. All experimental mice were anesthetized with 1.25% avertin (20 mg/kg; Sigma, USA). Pano2 cells were then digested with 0.25% trypsin and centrifuged at 1000 rpm for 4 min at 4 °C. The supernatant was removed, and the cells were resuspended with cold sterile PBS. Mice were carefully injected into the right flank with 5×10^6 Pano2 cells. After inoculation of the tumor for 10 days, the mice were randomly divided into three groups ($n = 5$ per group): Vehicle, CPPtat-S1 Control, and CPPtat-S1. Two days later, mice were subcutaneously administered CPPtat-S1 Control (10 mg/kg) and CPPtat-S1 (10 mg/kg). The weight of the mice was measured every two days. Meanwhile, tumor volume was monitored and calculated according to the formula ($1/2 \times \text{length} \times \text{width}^2$). After treatment, the tumors were harvested for further experiments. At the same time, the tumors were weighed and photographed. We have complied with all relevant ethical regulations for animal use. All protocols had been approved by the Animal Care Committee of Wenzhou Medical University, China.

Acyl-biotin exchange palmitoylation assay

Briefly, the HA-tagged CD38 construct was transfected into HEK293T cells. After two days, the cells were lysed using NP-40 lysis buffer containing the Protease Inhibitor Cocktail (EDTA-Free, 100X in DMSO) and 50 mM NEM (N-ethylmaleimide) on a rotator at 4 °C for 2 h. The supernatant was collected after centrifuging (10,000 rpm at 4 °C for 10 min). The supernatant obtained was then incubated with HA beads (bimake, China) to purify HA-CD38 at room temperature for 2 h. After purified treatment, beads were suspended with lysis buffer pH 7.2 and divided into two groups: -HAM (hydroxylamine) (Sigma-Aldrich) group (without HAM solution) and the +HAM group (with HAM solution). Next, the two groups were incubated at room temperature on a rotator for 1 h. The beads were washed three times with lysis buffer pH 7.2 and lysis buffer pH 6.2, respectively. Subsequently, the beads were incubated with 2 μM Biotin-HPDP (Thermo Fisher Scientific Inc.) for 1 h at 4 °C and then washed with lysis buffer pH 6.2. The beads were then boiled at 95 °C for 10 min after resuspending in 1× SDS-PAGE loading buffer (Beyotime, China). Finally, the palmitoylation level of CD38 was detected by immunoprecipitation of Streptavidin-HRP.

Co-immunoprecipitation assay

Cells were lysed with NP-40 buffer (Beyotime, China) including 1% protease inhibitor on ice for 10 min, and the lysate was centrifuged at 10,000 rpm for 10 min at 4 °C. The supernatant was reserved to avoid sucking to the bottom of the tube. The primary antibody and the corresponding supernatant were added together and incubated overnight at 4 °C on a rotator. The next day, the protein A/G agarose beads (Thermo Fisher Scientifific) were washed with TBST twice in advance according to the instructions and were then added to the supernatant containing antibodies and incubated at room temperature for another 4 h. Subsequently, the beads were collected using a magnetic rack (Thermo Fisher Scientifific) and resuspended in 50 μL 1× SDS-PAGE loading buffer. Finally, after the boiling the beads were for 10 min at 95 °C, the loading buffer was collected for western blotting detection.

Statistics and reproducibility

All data were presented as means ± standard Error (SEM). The above statistical analyses were carried out using one-way ANOVA with Tukey's correction (for comparisons of more than three groups) and Student's t-test (for comparisons between two groups). GraphPad Prism 8.0 software (GraphPad, San Diego, CA, USA) was used to perform the analyses and statistical significance was expressed as $^*p < 0.05$, $^{**}p < 0.01$, $^{***}p < 0.001$, or ns (ns not significant).

Data availability

The data supporting the findings of this study are included in the figures and Supplementary files. The source data behind the graphs in the paper are provided in Supplementary Data 1. All data are available from the corresponding authors upon reasonable request.

Received: 18 August 2024; Accepted: 6 March 2025;
Published online: 22 March 2025

References

1. Camacho-Pereira, J. et al. CD38 Dictates Age-Related NAD Decline and Mitochondrial Dysfunction through an SIRT3-Dependent Mechanism. *Cell Metab.* **23**, 1127–1139 (2016).
2. Chini, C. C. S. et al. CD38 ecto-enzyme in immune cells is induced during aging and regulates NAD(+) and NMN levels. *Nat. Metab.* **2**, 1284–1304 (2020).
3. Guerreiro, S., Privat, A. L., Bressac, L. & Toulorge, D. CD38 in Neurodegeneration and Neuroinflammation. *Cells* https://doi.org/10.3390/cells9020471 (2020).
4. Jin, D. et al. CD38 is critical for social behaviour by regulating oxytocin secretion. *Nature* **446**, 41–45 (2007).
5. Chini, E. N., Chini, C. C. S., Espindola Netto, J. M., de Oliveira, G. C. & van Schooten, W. The Pharmacology of CD38/NADase: an emerging target in cancer and diseases of aging. *Trends Pharm. Sci.* **39**, 424–436 (2018).
6. Konen, J. M., Fradette, J. J. & Gibbons, D. L. The Good, the Bad and the Unknown of CD38 in the Metabolic Microenvironment and Immune Cell Functionality of Solid Tumors. *Cells* https://doi.org/10.3390/cells9010052 (2019).
7. Gao, L., Du, X., Li, J. & Qin, F. X. Evolving roles of CD38 metabolism in solid tumour microenvironment. *Br. J. Cancer* **128**, 492–504 (2023).
8. Malavasi, F. et al. Evolution and function of the ADP ribosyl cyclase/CD38 gene family in physiology and pathology. *Physiol. Rev.* **88**, 841–886 (2008).

9. Hogan, K. A., Chini, C. C. S. & Chini, E. N. The Multi-faceted Ecto-enzyme CD38: Roles in Immunomodulation, Cancer, Aging, and Metabolic Diseases. *Front. Immunol.* **10**, 1187 (2019).
10. Chini, E. N. CD38 as a regulator of cellular NAD: a novel potential pharmacological target for metabolic conditions. *Curr. Pharm. Des.* **15**, 57–63 (2009).
11. Piedra-Quintero, Z. L., Wilson, Z., Nava, P. & Guerau-de-Arellano, M. CD38: An Immunomodulatory Molecule in Inflammation and Autoimmunity. *Front. Immunol.* **11**, 597959 (2020).
12. van de Donk, N. & Usmani, S. Z. CD38 antibodies in multiple myeloma: mechanisms of action and modes of resistance. *Front. Immunol.* **9**, 2134 (2018).
13. Lokhorst, H. M. et al. Targeting CD38 witH daratumumab monotherapy in multiple myeloma. *N. Engl. J. Med.* **373**, 1207–1219 (2015).
14. van de Donk, N., Richardson, P. G. & Malavasi, F. CD38 antibodies in multiple myeloma: back to the future. *Blood* **131**, 13–29 (2018).
15. Tirumurugaan, K. G. et al. TNF-alpha induced CD38 expression in human airway smooth muscle cells: role of MAP kinases and transcription factors NF-kappaB and AP-1. *Am. J. Physiol. Lung Cell Mol. Physiol.* **292**, L1385–L1395 (2007).
16. Guedes, A. G. et al. Role of CD38 in TNF-alpha-induced airway hyperresponsiveness. *Am. J. Physiol. Lung Cell Mol. Physiol.* **294**, L290–L299 (2008).
17. Murtadha, M. et al. CD38-directed, single-chain T cell-engager targets leukemia stem cells through IFNgamma-induced CD38 expression. *Blood* https://doi.org/10.1182/blood.2023021570 (2024).
18. Angelicola, S. et al. IFN-gamma and CD38 in hyperprogressive cancer development. *Cancers (Basel)* https://doi.org/10.3390/cancers13020309 (2021).
19. Musso, T. et al. CD38 expression and functional activities are up-regulated by IFN-γ on human monocytes and monocytic cell lines. *J. Leukoc. Biol.* **69**, 605–612 (2001).
20. Matalonga, J. et al. The nuclear receptor LXR limits bacterial infection of host macrophages through a mechanism that impacts cellular NAD metabolism. *Cell Rep.* **18**, 1241–1255 (2017).
21. Liu, Z. et al. Emerging roles of protein palmitoylation and its modifying enzymes in cancer cell signal transduction and cancer therapy. *Int. J. Biol. Sci.* **18**, 3447–3457 (2022).
22. Ko, P. J. & Dixon, S. J. Protein palmitoylation and cancer. *EMBO Rep.* https://doi.org/10.15252/embr.201846666 (2018).
23. Linder, M. E. & Deschenes, R. J. Palmitoylation: policing protein stability and traffic. *Nat. Rev. Mol. Cell Biol.* **8**, 74–84 (2007).
24. Hornemann, T. Palmitoylation and depalmitoylation defects. *J. Inherit. Metab. Dis.* **38**, 179–186 (2015).
25. Busquets-Hernandez, C. & Triola, G. Palmitoylation as a key regulator of Ras localization and function. *Front. Mol. Biosci.* **8**, 659861 (2021).
26. Chen, S. et al. Palmitoylation-dependent activation of MC1R prevents melanomagenesis. *Nature* **549**, 399–403 (2017).
27. Yao, H. et al. Inhibiting PD-L1 palmitoylation enhances T-cell immune responses against tumours. *Nat. Biomed. Eng.* **3**, 306–317 (2019).
28. Zhang, Z. et al. DHHC9-mediated GLUT1 S-palmitoylation promotes glioblastoma glycolysis and tumorigenesis. *Nat. Commun.* **12**, 5872 (2021).
29. Young, E. et al. Regulation of Ras localization and cell transformation by evolutionarily conserved palmitoyltransferases. *Mol. Cell Biol.* **34**, 374–385 (2014).
30. Ren, J. G. et al. RAB27B controls palmitoylation-dependent NRAS trafficking and signaling in myeloid leukemia. *J. Clin. Invest.* https://doi.org/10.1172/JCI165510 (2023).
31. Lin, Z. et al. Targeting ZDHHC9 potentiates anti-programmed death-ligand 1 immunotherapy of pancreatic cancer by modifying the tumor microenvironment. *Biomed. Pharmacother.* **161**, 114567 (2023).
32. Collins, M. O., Woodley, K. T. & Choudhary, J. S. Global, site-specific analysis of neuronal protein S-acylation. *Sci. Rep.* **7**, 4683 (2017).
33. Gould, N. S. et al. Site-specific proteomic mapping identifies selectively modified regulatory cysteine residues in functionally distinct protein networks. *Chem. Biol.* **22**, 965–975 (2015).
34. Shen, L. F. et al. Role of S-palmitoylation by ZDHHC13 in mitochondrial function and metabolism in liver. *Sci. Rep.* **7**, 2182 (2017).
35. Rusch, M. et al. Identification of acyl protein thioesterases 1 and 2 as the cellular targets of the Ras-signaling modulators palmostatin B and M. *Angew. Chem. Int. Ed. Engl.* **50**, 9838–9842 (2011).
36. Bu, L. et al. High-fat diet promotes liver tumorigenesis via palmitoylation and activation of AKT. *Gut* https://doi.org/10.1136/gutjnl-2023-330826 (2024).
37. Zaru, R. & Orchard, S. & UniProt, C. UniProt Tools: BLAST, align, peptide search, and ID mapping. *Curr. Protoc.* **3**, e697 (2023).
38. Ren, J. et al. CSS-Palm 2.0: an updated software for palmitoylation sites prediction. *Protein Eng. Des. Sel.* **21**, 639–644 (2008).
39. Ning, W. et al. GPS-Palm: a deep learning-based graphic presentation system for the prediction of S-palmitoylation sites in proteins. *Brief Bioinform.* **22**, 1836–1847 (2021).
40. Zhou, B., Hao, Q., Liang, Y. & Kong, E. Protein palmitoylation in cancer: molecular functions and therapeutic potential. *Mol. Oncol.* **17**, 3–26 (2023).
41. Gorleku, O. A., Barns, A. M., Prescott, G. R., Greaves, J. & Chamberlain, L. H. Endoplasmic reticulum localization of DHHC palmitoyltransferases mediated by lysine-based sorting signals. *J. Biol. Chem.* **286**, 39573–39584 (2011).
42. Lakkaraju, A. K. et al. Palmitoylated calnexin is a key component of the ribosome-translocon complex. *EMBO J.* **31**, 1823–1835 (2012).
43. Malgapo, M. I. P., Safadi, J. M. & Linder, M. E. Metallo-beta-lactamase domain-containing protein 2 is S-palmitoylated and exhibits acyl-CoA hydrolase activity. *J. Biol. Chem.* **296**, 100106 (2021).
44. Runkle, K. B. et al. Inhibition of DHHC20-Mediated EGFR Palmitoylation Creates a Dependence on EGFR Signaling. *Mol. Cell* **62**, 385–396 (2016).
45. Vujic, I. et al. Acyl protein thioesterase 1 and 2 (APT-1, APT-2) inhibitors palmostatin B, ML348 and ML349 have different effects on NRAS mutant melanoma cells. *Oncotarget* **7**, 7297–7306 (2016).
46. Wo, Y. J. et al. The roles of CD38 and CD157 in the solid tumor microenvironment and cancer immunotherapy. *Cells* https://doi.org/10.3390/cells9010026 (2019).
47. Jiao, Y. et al. CD38: targeted therapy in multiple myeloma and therapeutic potential for solid cancers. *Expert Opin. Investig. Drugs* **29**, 1295–1308 (2020).
48. Ge, Y. et al. CD38 affects the biological behavior and energy metabolism of nasopharyngeal carcinoma cells. *Int. J. Oncol.* **54**, 585–599 (2019).
49. Levy, A. et al. CD38 deficiency in the tumor microenvironment attenuates glioma progression and modulates features of tumor-associated microglia/macrophages. *Neuro Oncol.* **14**, 1037–1049 (2012).
50. Karakasheva, T. A. et al. CD38-expressing myeloid-derived suppressor cells promote tumor growth in a murine model of esophageal cancer. *Cancer Res.* **75**, 4074–4085 (2015).
51. Nijhof, I. S. et al. CD38 expression and complement inhibitors affect response and resistance to daratumumab therapy in myeloma. *Blood* **128**, 959–970 (2016).
52. Sun, Y. et al. S-palmitoylation of PCSK9 induces sorafenib resistance in liver cancer by activating the PI3K/AKT pathway. *Cell Rep.* https://doi.org/10.1016/j.celrep.2022.111194 (2022).
53. Mesquita, S. F. et al. Mechanisms and functions of protein S-acylation. *Nat. Rev. Mol. Cell Biol.* https://doi.org/10.1038/s41580-024-00700-8 (2024).
54. Haag, S. M. et al. Targeting STING with covalent small-molecule inhibitors. *Nature* **559**, 269–273 (2018).
55. Roboon, J. et al. Inhibition of CD38 and supplementation of nicotinamide riboside ameliorate lipopolysaccharide-induced

microglial and astrocytic neuroinflammation by increasing NAD(). *J. Neurochem* **158**, 311–327 (2021).
56. Hattori, T. et al. Postnatal expression of CD38 in astrocytes regulates synapse formation and adult social memory. *EMBO J.* **42**, e111247 (2023).
57. Covarrubias, A. J. et al. Senescent cells promote tissue NAD(+) decline during ageing via the activation of CD38(+) macrophages. *Nat. Metab.* **2**, 1265–1283 (2020).
58. Zhang, X. et al. The role of CD38 in inflammation-induced depression-like behavior and the antidepressant effect of (R)-ketamine. *Brain Behav. Immun.* **115**, 64–79 (2024).

Acknowledgements

We thank Professor Er-yan Kong (Xinxiang Medical University) for providing plasmids of APT1, APT2, ZDHHC4, ZDHHC6 and ZDHHC20. We thank Scientific Research Center of Wenzhou Medical University for providing excellent consultation and instrumental supports. This work was supported by the National Natural Science Foundation of China (Grant No. 31970948 to W.G.) the Scientific Research Starting Foundation of Wenzhou Medical University (Grant No. QTJ12003 to J.C.) and the Department of Science and Technology of Zhejiang Province (Grant No. 2023ZY1011 to J.C.).

Author contributions

H.G. and Z.-Q.L.: Conceptualization, Methodology, Investigation, Writing of the original draft. D.Z.: Methodology, Investigation. Q.-L.Q., Z.-W.L., and Y.-Q.Y.: Investigation. J.-F.C.: Funding acquisition, Supervision, Draft reviewing and editing. W.G.: Conceptualization, Data curation, Funding acquisition, Writing of the original draft, Draft reviewing and editing.

Competing interests

The authors declare no competing interests.

Additional information

Supplementary information The online version contains supplementary material available at https://doi.org/10.1038/s42003-025-07897-0.

Correspondence and requests for materials should be addressed to Jiangfan Chen or Wei Guo.

Peer review information *Communications Biology* thanks Binhui Zhou and the other, anonymous, reviewers for their contribution to the peer review of this work. Primary Handling Editors: Toshiro Moroishi and Mengtan Xing. A peer review file is available.